A Novel Controlled Frequency Band Impedance Measurement Approach for Single-Phase Railway Traction Power System

Haitao Hu, *Member, IEEE*, Pengyu Pan, *Student Member, IEEE*, Yitong Song, and Zhengyou He, *Senior Member, IEEE*

***Abstract*—The accurate information of the wide-bandwidth impedance versus the frequency is urgently needed for evaluating the system resonances, instabilities, and operations of the railway traction power system (TPS), and to avoid/control the harmonic resonance and oscillation issues. As the system topology and detailed parameters of the TPS are not fully known even timely varying, we have to obtain the detailed wide-bandwidth impedance information through exciting the harmonic disturbance into the system, and then, calculating the response information. Therefore, a controlled wide-bandwidth impedance measurement approach is presented in this paper, in which, a butterfly-type disturbance circuit and chirp pulsewidth modulation signal model are incorporated to generate the desired controlled-bandwidth harmonics with a high aggregation as well as the average amplitude. Impedance measurement results of the proposed approach have been validated through both simulation and experiment. Considering the measured errors, the proposed method is efficient in testing the wide-bandwidth impedance of the single-phase railway traction system.**

***Index Terms*—Controlled harmonic excitation, harmonic resonance, impedance measurement, railway traction power system (TPS).**

I. Introduction

TRACTION power system is a significant part of the electric railway system that delivers the power from the utility power system to electric trains [1]–[3]. Previous publications pointed out that the impedance of the traction system largely affects the operation and control of the electric train [4]–[8]. The instability problems (e.g., harmonic resonance and low-frequency oscillation) have frequently occurred and reported around the world due to the impedance mismatch of the train and traction network system (hereinafter, train-network system) [5]. One effective solution is improving the electric train control according to the specific traction network impedance [9]–[12]. The harmonic resonance points or instable damping information can be obtained according to the system impedance. As a result, the corresponding mitigation schemes in terms of filters and control parameter optimization can be applied, and the harmonic resonances and instabilities can be greatly reduced for guaranteeing the safety and stability of the TPS.

However, solely utilizing the mathematical deduction to estimate the impedance seems to be difficult and inaccurate owing to unknown detailed parameters of the TPS and its complicated mathematical process. Therefore, the impedance measurement technique is required to obtain the TPS impedance.

There are two conventional categories of methods for the grid impedance measurement on the basis of exciting disturbance, i.e., internal system operation disturbance [13] and additional disturbance [14] by means of connecting devices. In order to obtain the accurate and reliable grid impedance, additional disturbance methods are more popular and reliable. Furthermore, to reduce the injection times of the disturbance, wide-bandwidth impedance measurement approaches have been paid more concern [15], [18]–[21]. Nevertheless, wide-bandwidth disturbance, being applied to measure the impedance, should address the following three key technologies.

1) The frequencies of exciting the wide-bandwidth disturbance should be controllable and with enough power that can acquire accurate response under an actual noise environment.
2) The amplitude values of exciting harmonics at different frequencies should be averaged and approximately same, and can be controlled. It saves the required power of the disturbance circuit and avoids the effect of the excessive injection.
3) The disturbance should not affect the normal operations of the power system. It is needed to limit the disturbance power of each frequency, which is contradictory with the first one.

Existing impedance measurement techniques, such as the sinusoidal waveform sweep-based method in [16] and [17], produce the promising signal-to-noise ratio to measure the accurate impedance. Nevertheless, the sinusoidal waveform

Manuscript received September 19, 2018; revised December 11, 2018; accepted January 10, 2019. Date of publication February 5, 2019; date of current version August 30, 2019. This work was supported in part by the National Natural Science Foundation of China under Grant NSFC 51677154 and Grant 51525702, and in part by the Young Elite Scientists Sponsorship Program by CAST under Grant YESS 2017QNRC001. (*Corresponding author: Haitao Hu.*)

The authors are with the School of Electrical Engineering, Southwest Jiaotong University, Chengdu 614202, China (e-mail: hht@swjtu.edu.cn; ppyswjtu@163.com; yitong_song@ 163.com; hezy@swjtu.edu.cn).

Color versions of one or more of the figures in this paper are available online at http://ieeexplore.ieee.org.

Digital Object Identifier 10.1109/TIE.2019.2896297

sweep method needs more time to generate different frequency injections repeatedly and compute the impedance information using the frequency scan. The random pulsewidth modulation (PWM) signal is presented in [18], and the grid impedance can be measured over a wide bandwidth through only single injection so that the measurement time is greatly shortened. However, this excited frequency band is not controllable.

Dr. Roinila has done some meaningful researches on the pseudo-random binary sequences, such as the maximum-length binary sequence [19], [20] and discrete-interval binary sequence [21]. They can give an adjustable harmonic excitation relying on the grid-connected converters. Using the small-power chirp signal introduced in [22]–[24] can detect the bioelectrical impedance, but is futile for the large-power/capacity electric grid. Thus, a method for producing the large-power chirp signal is proposed in [25], but that makes the voltage disturbance connecting to the grid in series, being not practical for the railway system.

Therefore, a novel impedance measurement approach for the TPS is presented here. The disturbance circuit along with the chirp-PWM signal being connected to the TPS in parallel is more practical to measure the wide-bandwidth impedances. The main contributions of this paper are listed as follows.

1) A butterfly-type disturbance circuit is designed to produce the wide-bandwidth harmonic excitation. The circuit is simple and only few switching devices are required.
2) The chirp-PWM used in the impedance measurement has been derived. The disturbance circuit is controlled by the given chirp-PWM signal so that the injected frequency spectrum can be easily controlled.
3) We have defined three indices, namely, harmonic concentration ratio (HCR), harmonic distribution uniformity (HDU), and harmonic frequency resolution (HFR), to evaluate the performance of the harmonic excitation. These indices help us to focus on the injection power at the desired frequencies or bandwidth for the accurate and efficient measurement.

In order to validate the performance and practicality of the presented approach, impedance measurement results of the proposed approach have been conducted according to simulation and experiment. The rest of this paper is organized as follows. An impedance measurement strategy for the TPS is introduced in Section II. Section III presents the method to produce harmonic injection at controlled frequency band. Thus, a simulation measurement for the TPS is presented and discussed in detail in Section IV. Section V shows the experimental validation. Finally, Section VI concludes this paper.

II. Impedance Measurement for the TPS

The TPS is a typical single-phase industrial power system, in which, the traction transformer steps down the high voltage of the three-phase utility power system to two single-phase 27.5-kV voltages to supply electric trains. The auto transformer (AT)-fed catenary system [2], [26] is widely applied in the high-speed railways around the world, as illustrated in Fig. 1. The

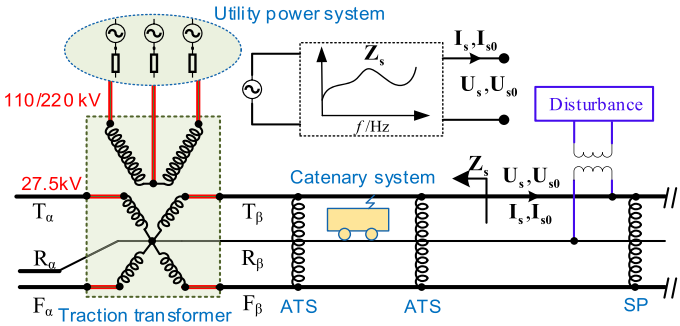

Fig. 1. TPS with AT catenary system.

traction system contains the utility grid, traction transformer, and the catenary system including contact wires (T_α, T_β), rails (R_α R_β), and positive feeders (F_α, F_β). It should be noted that the measurement will be conducted without running trains in order to obtain the accurate harmonic impedances of the TPS. The impedance measurement of the modern electric trains, characterizing different behaviors and disturbance modes, is not described in this paper. With considering the frequency coupling, the method can be found in our previous work [27].

When the TPS operates without additional disturbances, the self-generated harmonics existed in the system can be applied to compute the impedance only versus the corresponding frequencies. The more desired harmonics excited by the disturbance can be applied for detecting the more complete impedance. If the excited harmonics can be controlled, the frequency band of the measured impedance is controllable.

In the actual measurement, the background harmonics should be considered to guarantee the accuracy of the measurement [27]. The voltage $\mathbf{U_{s0}}$ and current $\mathbf{I_{s0}}$ of the TPS are measured first without imposing disturbances, which also comprises of background harmonic frequencies besides the fundamental frequency. Then, the disturbance circuit is connected to the TPS for measuring the response voltage $\mathbf{U_s}$ and current $\mathbf{I_s}$ with a desired frequency band. Finally, fast Fourier transform (FFT) is adopted to obtain the frequency-domain components of the measured data, and the impedance can be calculated by

$$\mathbf{Z_s}(j\omega) = \frac{\mathbf{U_s}(j\omega) - \mathbf{U_{s0}}(j\omega)}{\mathbf{I_s}(j\omega) - \mathbf{I_{s0}}(j\omega)} \tag{1}$$

where $\mathbf{U_{s0}}(j\omega)$ and $\mathbf{I_{s0}}(j\omega)$ are the voltage and current of the TPS without imposing the disturbance in the frequency domain, respectively; and $\mathbf{U_s}(j\omega)$ and $\mathbf{I_s}(j\omega)$ are the response voltage and current after imposing the disturbance, respectively.

III. Disturbance Injection at a Controlled Frequency Band

A. Chirp-PWM Signal

The chirp signal, one of the common wide-bandwidth signals, is a sinusoidal waveform signal possessing the time-varying frequency [22]–[25]. It is widely used in signal transmission, such as the radar system. The linear chirp waveform owning the

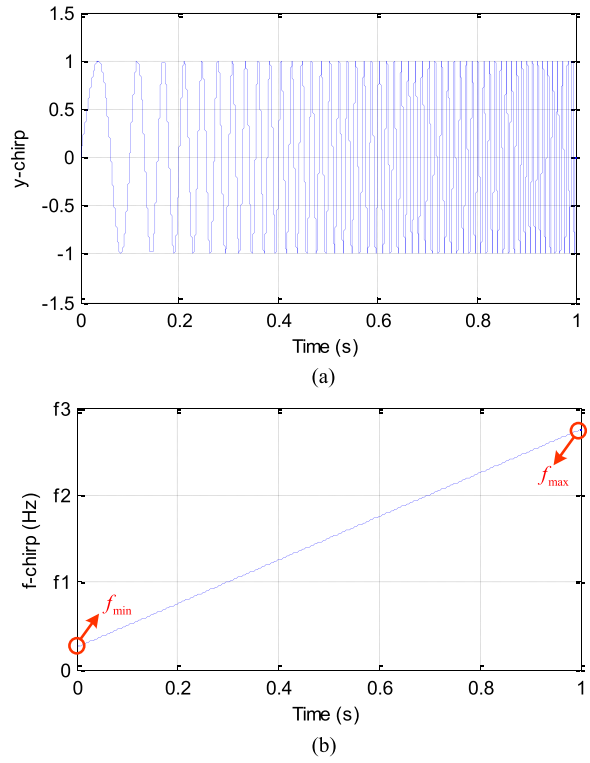

Fig. 2. Typical linear chirp signal with a frequency band from $f_{\min}$ to $f_{\max}$. (a) Waveform in time domain. (b) Frequency of this chirp signal.

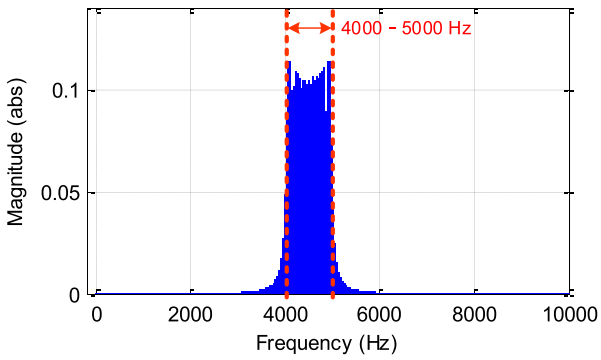

Fig. 3. Harmonic spectrum of a chirp signal with a specified frequency band from 4000 to 5000 Hz.

linear time-varying frequency is given by

$$y_{\text{chirp}}(t) = \sin\left\{2\pi t\left[f_{\min} + (f_{\max} - f_{\min})\frac{t}{2T}\right]\right\} \quad (2)$$

where $f_{\min}$ and $f_{\max}$ are the specified minimum and maximum frequencies, respectively; and T is the duration of the linear chirp waveform. Seen from (2), the instantaneous frequency of the linear chirp can be written as

$$f_{\text{chirp}}(t) = f_{\min} + (f_{\max} - f_{\min})\frac{t}{T}. \quad (3)$$

The specified frequency $f_{\min}$ and $f_{\max}$ can control the spectrum at the desired frequency band. A typical linear chirp signal shown in Fig. 2 is employed to describe (2) and (3) clearly.

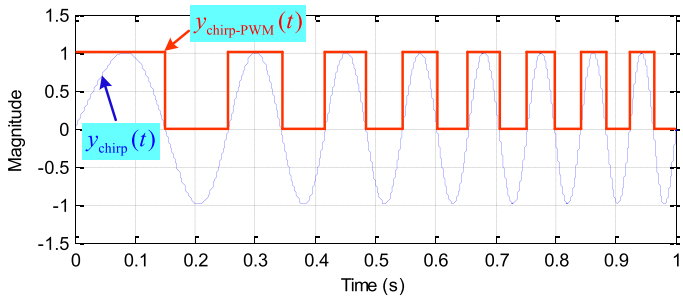

Fig. 4. Converting scheme of chirp signal to chirp-PWM signal.

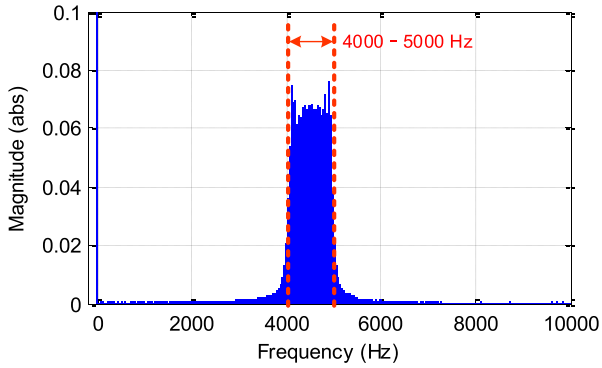

Fig. 5. Spread frequency spectrum of a chirp-PWM signal with a specified frequency band from 4000 to 5000 Hz.

The frequency spectrum of the chirp signal, setting and increasing its bandwidth from the initial 4000 to 5000 Hz in 1 s, is presented in Fig. 3. One can find that the spread frequency spectrum can distribute the harmonic power over the specified frequency band 4000–5000 Hz satisfactorily.

As a novel PWM scheme, the chirp-PWM proposed in [28] has various switching frequencies with a chirp feature instead of fixing (as in [27]) or randomizing (as in [18]) the switching frequencies for the classical PWM scheme. To adapt the aforementioned linear chirp signal $y_{\text{chirp}}(t)$ to PWM-type (i.e., chirp-PWM) signal, an effective converting scheme $y_{\text{chirp-PWM}}(t)$ can be actualized as

$$y_{\text{chirp-PWM}}(t) = \begin{cases} 1, & y_{\text{chirp}}(t) \geq 0 \\ 0, & y_{\text{chirp}}(t) < 0 \end{cases}. \quad (4)$$

The aforementioned equation illustrates that the converting scheme switches the chirp signal to "1" as the chirp value is larger than 0 (i.e., $y_{\text{chirp}}(t) \geq 0$), and for another state, chirp signal with a value smaller than 0 (i.e., $y_{\text{chirp}}(t) < 0$) should be switched to "0." The detailed converting scheme can be seen in Fig. 4.

The spread frequency spectrum of a chirp-PWM signal, e.g., controlling its frequency band at the same 4000–5000 Hz, is shown in Fig. 5. It illustrates that the actual frequency spectrum can also spread at the specified frequency band 4000–5000 Hz. The chirp-PWM signal, usually being obtained by the micro controller unit (MCU), just has a low power and seems to be futile to detect the impedance of the large-power/capacity TPS. To excite a harmonic disturbance at a specified frequency band with

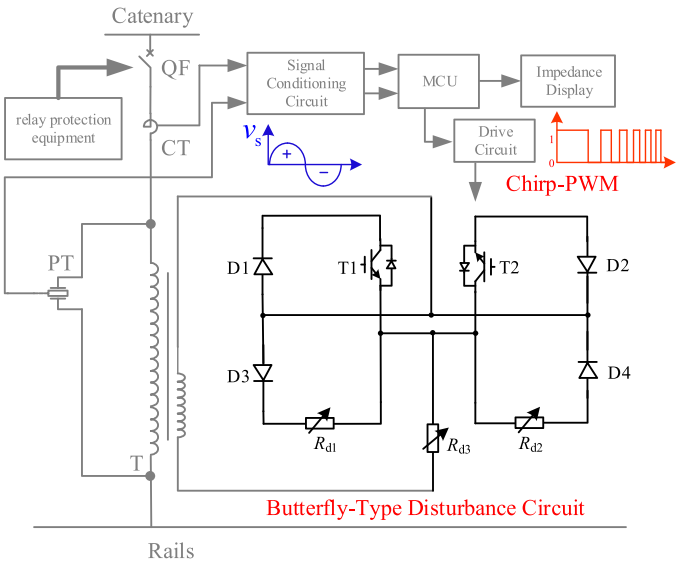

Fig. 6. Butterfly-type disturbance circuit to produce the harmonic disturbance in the TPS.

a large power into the TPS to detect the system impedance, the chirp-PWM signal is adopted to drive the insulated-gate bipolar transistor (IGBT) of the proposed butterfly-type disturbance circuit presented in following subsection.

B. Butterfly-Type Disturbance Circuit

The butterfly-type circuit with two controllable switches is illustrated in Fig. 6 to produce the harmonic disturbance with a large power in the TPS. The circuit contains two IGBTs (T1 and T2), four uncontrollable diodes (D1, D2, D3, and D4), and three adjustable resistors (R_{d1}, R_{d2}, and R_{d3}). The voltage sensor (PT) and current sensor (CT) can detect the response data for impedance calculation by the MCU that can also generate the chirp-PWM signal to drive the IGBTs of the butterfly-type circuit.

The proposed disturbance circuit has four topological stages, which are shown in detail in Fig. 7. Two of these four stages are for the positive cycle of the input voltage v_s, in which the current flows through the black circuit pointed by the red dotted line detailed in Fig. 7(a) (IGBTs get an instruction "ON") and Fig. 7(b) (IGBTs get an instruction "OFF"). The other two topological states are for the negative cycle and are similar to those for the positive cycle, and the current flows through the black circuit detailed in Fig. 7(c) (IGBTs get an instruction "ON") and Fig. 7(d) (IGBTs get an instruction "OFF").

In the first topological stage seen in Fig. 7(a), the controllable IGBTs are turned ON and only the resistor R_{d3} is fed in the black circuit loop (pass through D1, T1, and R_{d3} successively), which causes a resulted current v_s/R_{d3} for the positive cycle of the input voltage v_s.

The second topological stage seen in Fig. 7(b) starts when the controllable IGBTs are turned OFF; hence, both the resistor R_{d1} and R_{d3} are fed together in the black circuit loop (pass through D3, R_{d1}, and R_{d3} successively), resulting in a response current $v_s/(R_{d1}+R_{d3})$ for the positive cycle of v_s.

The other two topological stages for the negative cycle of v_s are similar to the stages of the positive cycle and are shown in Fig. 7(c) and (d), respectively.

In steady-state operations, the response current detailed in Fig. 8 going across all the four topological stages repeatedly are v_s/R_{d3}, $v_s/(R_{d1}+R_{d3})$, v_s/R_{d3}, and $v_s/(R_{d2}+R_{d3})$, respectively. The iterative four stages generate some gaps with a chirp-PWM feature on the response current, which can provide harmonic disturbance at a specified frequency band for the TPS.

The resistors R_{d1} and R_{d2} inside the arms of the butterfly-type disturbance circuit and R_{d3} outside the arms quantify the gap depth of the response current that$(R_{d1}+R_{d3})/R_{d3}$ (i.e., $R_{d1}/R_{d3}+1$) for the positive cycle and $(R_{d2}+R_{d3})/R_{d3}$ (i.e., $R_{d2}/R_{d3}+1$) for the negative cycle. It indicates that larger ratio of R_{d1}/R_{d3} and R_{d2}/R_{d3} can facilitate the deeper gap on the response current.

Fig. 9 presents the spread frequency spectrum of the response current for a given case with a specified frequency band at 4000–5000 Hz. The actual frequency spectrum spread exactly matches the specified frequency band from 4000 to 5000 Hz with the other harmonics having a tiny amplitude, which validates the effectiveness of the proposed disturbance method. Besides harmonic components, it is noteworthy that the fundamental component accounts majority of the injection power due to the fundamental waveform-based distortion. There are some filtering solutions to control the injection of the fundamental component [29].

The proposed measurement equipment is connected to the catenary of the TPS in parallel, and a circuit breaker (QF) and corresponding relay protection equipment are installed at the input terminal of the measurement equipment, as shown in Fig. 6. The corresponding protection strategies (e.g., current protection, overload protection, and differential protection) can be set to protect both TPS and measurement equipment.

C. Evaluating Indices of Harmonic Disturbance

In order to evaluate the harmonic disturbance at a specified frequency band for impedance measurement, three indices in terms of disturbance injection are given as follows.

1) Harmonic Concentration Ratio (HCR): HCR characterizes the proportion of the excited harmonics at a specified frequency band to the full band, which can be described by

$$\mathrm{HCR}=\frac{\sum_{x=f_{\min}}^{f_{\max}} I^2(x)}{\sum_{x=f_{\mathrm{MIN}}}^{f_{\mathrm{MAX}}} I^2(x)} \tag{5}$$

where $I(x)$ is the excited harmonic current by the disturbance circuit; and f_{MIN} and f_{MAX} are the minimum and maximal frequency of the full frequency band, respectively. A larger value of the HCR characterizes a more centralized spread frequency spectrum, and thus, gives a more suitable harmonic disturbance for impedance measurement at the specified frequency band.

2) Harmonic Distribution Uniformity (HDU): HDU, being defined to evaluate the uniformity for the excited harmonics at

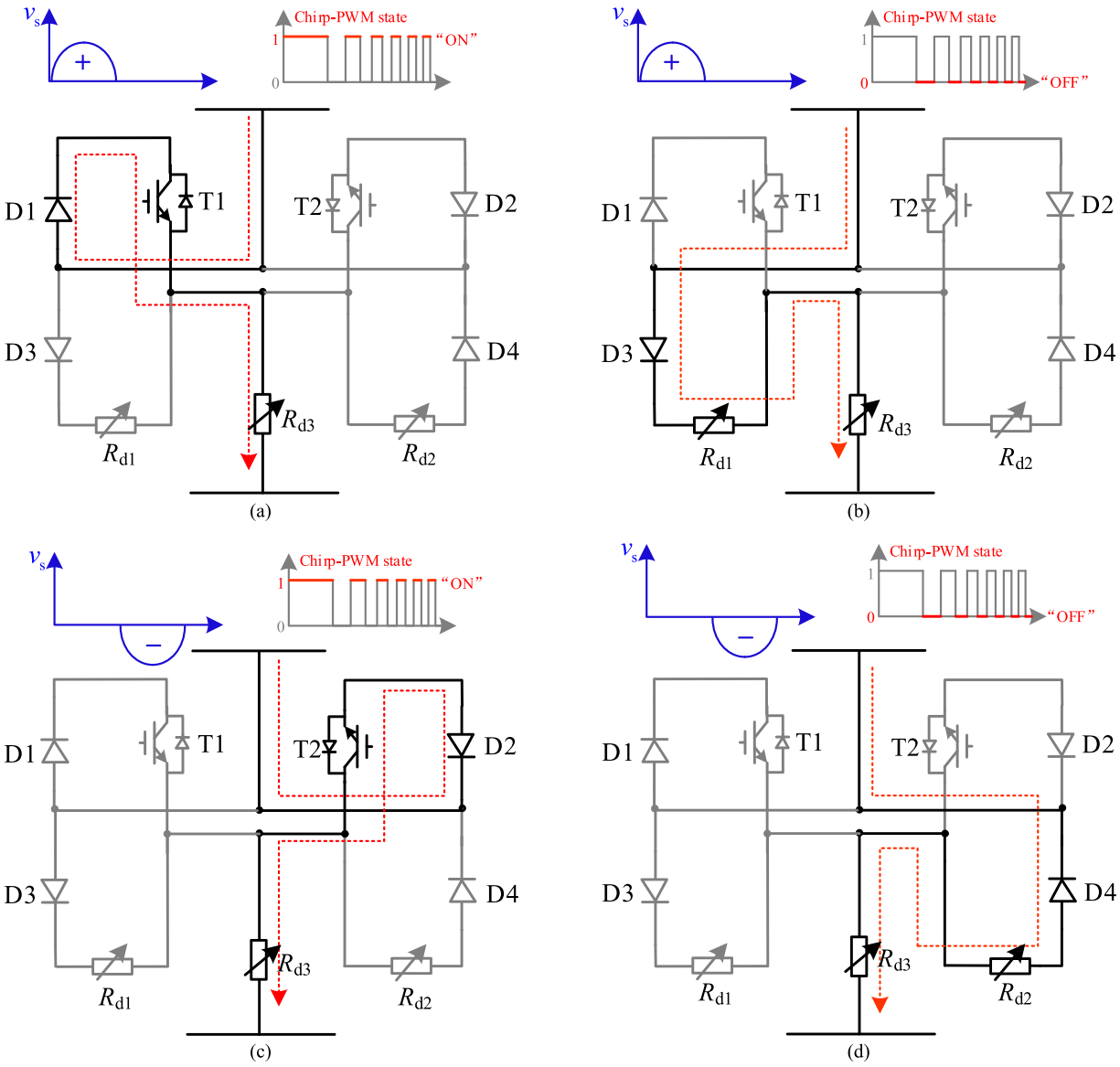

Fig. 7. Four topological stages of the proposed disturbance circuit. (a) First stage for the positive cycle of the input voltage when IGBTs get "ON." (b) Second stage for the positive cycle of the input voltage when IGBTs get "OFF." (c) Third stage for the negative cycle of the input voltage when IGBTs get "ON." (d) Fourth stage for the negative cycle of the input voltage when IGBTs get "OFF."

a specified frequency band, is given by

$$\mathrm{HDU} = \frac{\sigma^2}{\sum_{x=f_{\min}}^{f_{\max}} I^2(x)/N} \tag{6}$$

where N is the sampling number; and σ^2 is the variance of excited harmonic currents at the specified frequency band and it can be described by

$$\sigma^2 = \frac{\sum_{x=f_{\min}}^{f_{\max}} [I(x) - \mu]^2}{N} \tag{7}$$

where μ is the mean value of excited harmonic currents at a specified frequency band and can be obtained by

$$\mu = \frac{\sum_{x=f_{\min}}^{f_{\max}} |I(x)|}{N}. \tag{8}$$

A smaller HDU characterizes a more uniform spread frequency spectrum at the specified frequency band, which will give a more accurate measurement result. The reason is that a uniform spread frequency spectrum indicates that the magnitudes of injected harmonics have the similar values, and there are no or less relatively small harmonic magnitudes occurring to the injected harmonics.

3) Harmonic Frequency Resolution (HFR): FFT being applied to extract the information in frequency domain from the time-domain data can give an HFR as

$$\mathrm{HFR} = \frac{1}{t} \tag{9}$$

where t is the time of the chirp-PWM signal in a periodical sinusoidal waveform shown in Fig. 8. One can control the

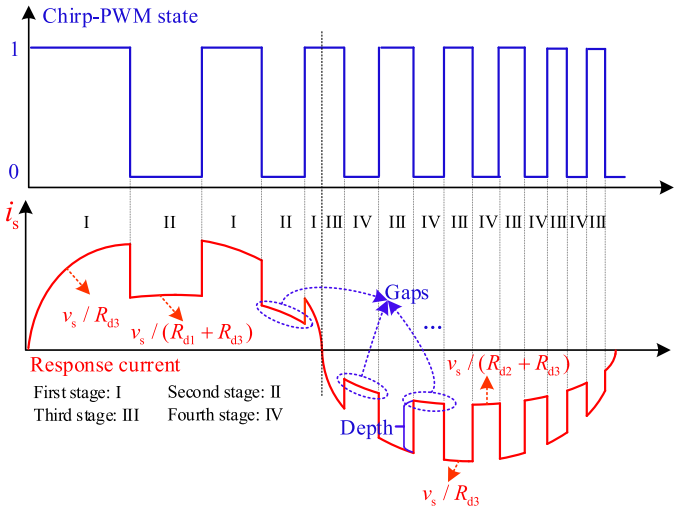

Fig. 8. Response current after disturbance.

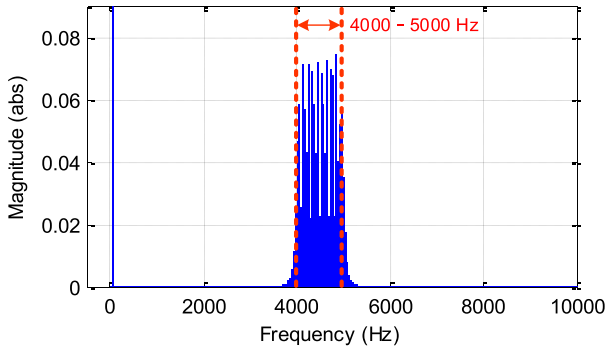

Fig. 9. Spread frequency spectrum produced by the disturbance circuit with a specified frequency band from 4000 to 5000 Hz.

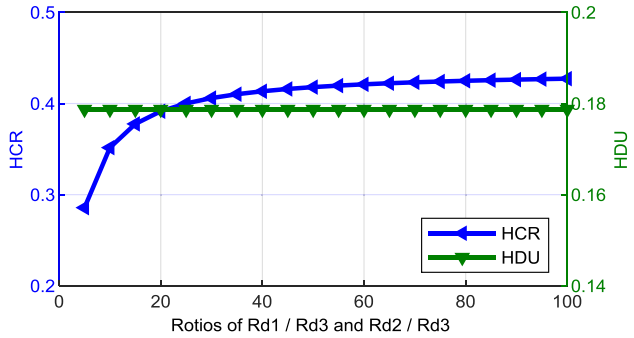

Fig. 10. HCR and HDU for the varying ratios of R_{d1}/R_{d3} and R_{d2}/R_{d3}.

HFR through controlling the duration time of a complete chirp-PWM signal. The HFR represents the frequency resolution of the impedance.

The two indices HCR and HDU, reported in Fig. 10 with different ratios of R_{d1}/R_{d3} and R_{d2}/R_{d3}, indicate that the HCR has a upward trend without deteriorating the HDU along with increasing the ratios of R_{d1}/R_{d3} and R_{d2}/R_{d3}. Thus, for the disturbance circuit design, the ratios of R_{d1}/R_{d3} and R_{d2}/R_{d3} would better be large (50 is the best) to bring a highly centralized

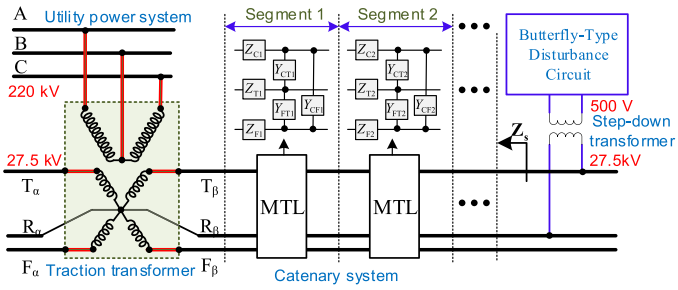

Fig. 11. Schematic of the TPS simulation model using MTL.

TABLE I
SIMULATION PARAMETERS FOR THE TPS

Parameter	Value
Utility power system voltage	220 kV
Connection of traction transformer	V/x
Voltage ratio of traction transformer	220 kV/27.5 kV
Primary side parameters of traction transformer	3.46 Ω, 255 mH
Secondary side parameters of traction transformer	0.054 Ω, 3.98 mH
The number of segments	10
Voltage ratio of step-down transformer	27.5 kV/500 V
R_{d1} of butterfly-type disturbance circuit	5000 Ω
R_{d2} of butterfly-type disturbance circuit	5000 Ω
R_{d3} of butterfly-type disturbance circuit	100 Ω
ratios of R_{d1} / R_{d3} and R_{d2} / R_{d3}	50

spread frequency spectrum at a specified frequency band, which would be appropriate for the impedance measurement.

The third indicator the HFR being related to the sampling time can be confirmed according to the actual measurement requirement of the frequency resolution, and the sampling time should be larger when the requirement of the frequency resolution is higher.

IV. Simulation Result of the Impedance Measurement at a Controlled Frequency Band

A. Simulation Model

In order to validate the effectiveness of the proposed measurement approach, a detailed TPS is considered as the test system. The catenary system, being regarded as one symmetrical linear and passive multiport network, is built in MATLAB/SIMULINK based on the multiple transmission line (MTL) model [5]. The schematic of the TPS simulation model using the MTL is given in Fig. 11.

The MTL unit represents the segment of different lengths of the catenary system. As to detect the impedance at different location of the catenary system, the proposed disturbance circuit should disturb the different segments to excite the harmonic disturbance.

B. Simulation Results

The simulation parameters are given in Table I. The voltage of the utility power system is 220 kV being transformed

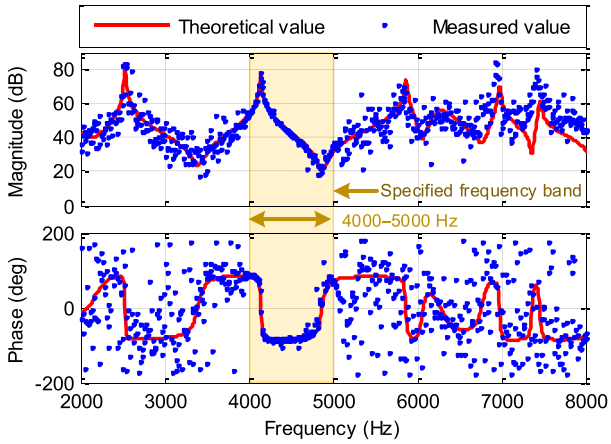

Fig. 12. Measured TPS impedance when the specified frequency band is 4000–5000 Hz.

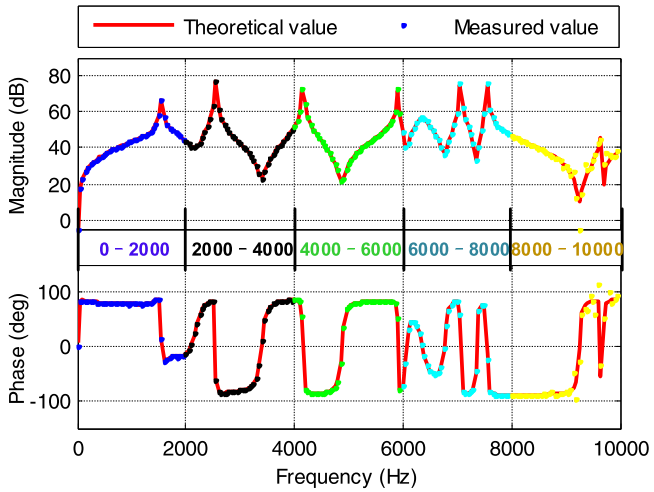

Fig. 13. Measured TPS impedance when the specified frequency band is 0–10000 Hz with 2000-Hz measurement interval.

to 2 × 27.5 kV by the traction transformer for supplying the catenary system. The simulation time step is set as $T_s = 1 \times 10^{-6}$ s. For a given case, the specified frequency band is set as 4000–5000 Hz and the measured results are shown in Fig. 12. The impedance extracted from the simulation measurement at the specified frequency band 4000–5000 Hz (the yellow region) is almost consistent with the theoretical value and that out of the specified frequency band is inaccurate since there is no enough harmonic excitation at these frequencies. Considering the exorbitant harmonic excitation may affect the normal operation of the TPS, in order to measure the TPS impedance at a broader band, 0–10 000 Hz, for example, we can conduct a segmental measurement every 2000 Hz (i.e., 0–2000 Hz, 2000–4000 Hz, 4000–6000 Hz, 6000–8000 Hz, and 8000–10 000 Hz), as shown in Fig. 13. The measured impedance at a specified frequency band can be detected accurately to validate the effectiveness of the proposed measurement method.

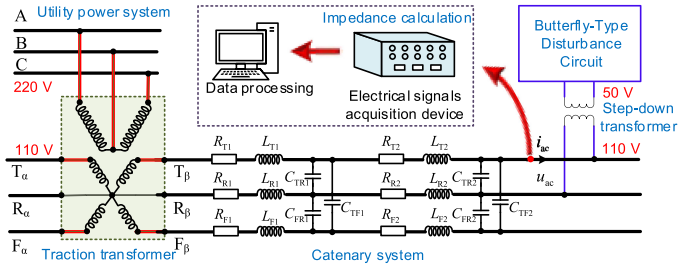

Fig. 14. Diagram of the impedance measurement.

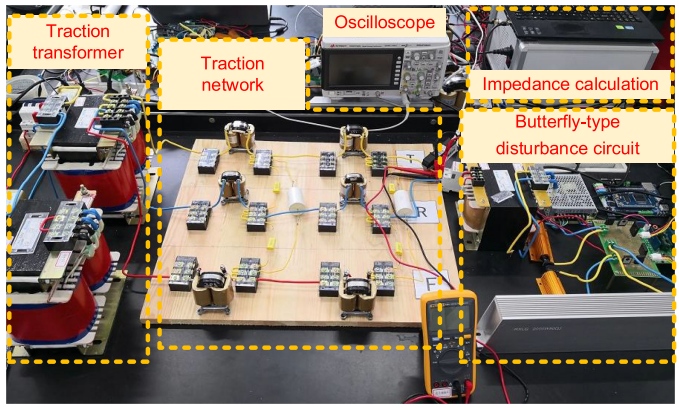

Fig. 15. Experimental device of the impedance measurement.

TABLE II
IMPENDENCE MEASUREMENT EXPERIMENTAL SYSTEM PARAMETERS

Parameter	Value
Actual utility power system voltage	230 V
Connection of traction transformer	V/x
Rated voltage ratio of traction transformer	220 V/110 V
Primary side parameters of traction transformer	0.3 Ω, 289 mH
Secondary side parameters of traction transformer	0.2 Ω, 73 mH
Contact wire resistor	R_{T1}=0.1 Ω; R_{T2}=0.1 Ω
Contact wire inductor	L_{T1}=2 mH; L_{T2}=2 mH
Track resistor	R_{R1}=0.2 Ω; R_{R2}=0.2 Ω
Track inductor	L_{R1}=1 mH; L_{R2}=1 mH
Negative feeder resistor	R_{F1}=0.1 Ω; R_{F2}=0.1 Ω
Negative feeder inductor	L_{F1}=2 mH; L_{F2}=2 mH
Catenary system capacitor	C_{TR1}=1.5 uF; C_{FR1}=1.5 uF; C_{TF1}=3 uF; C_{TR2}=1.5 uF; C_{FR2}=1.5 uF; C_{TF2}=3 uF
Rated voltage ratio of step-down transformer	110 V/50 V
R_{d1} of butterfly-type disturbance circuit	100 Ω
R_{d2} of butterfly-type disturbance circuit	100 Ω
R_{d3} of butterfly-type disturbance circuit	50 Ω

V. EXPERIMENTAL VALIDATION

A. Experimental Setup

An experimental system including the disturbance circuit, shown in Figs. 14 and 15, is conducted to validate the practicality and capability of the impedance measurement approach, and the electric parameters of the experimental system are listed in Table II. The TPS model is built referring to the actual engineering structure including the utility power system, V/x-type traction transformer, and catenary system. A DSP 28335 control system selected as an MCU can provide the chirp-PWM signal to control the IGBTs of the butterfly-type disturbance circuit,

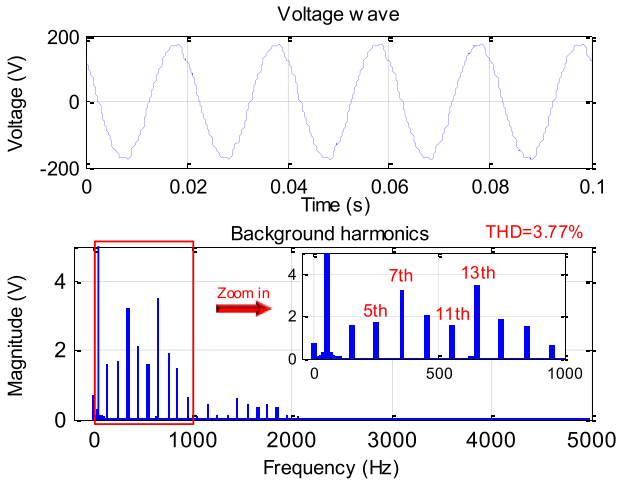

Fig. 16. Background voltage waveform and its harmonic spectrum without disturbance.

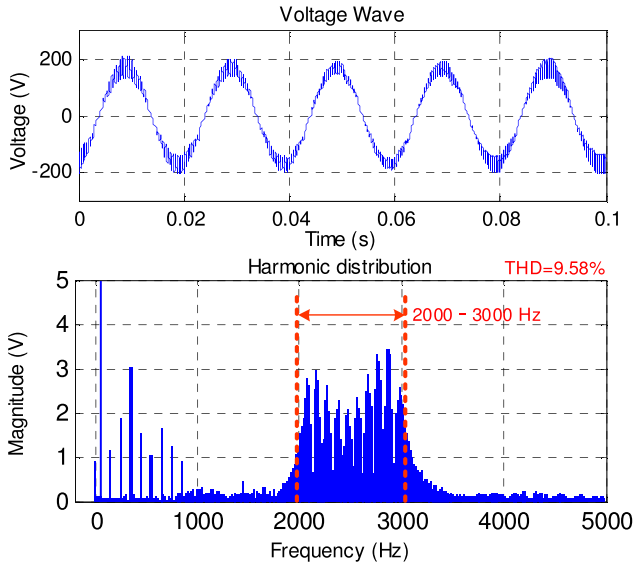

Fig. 17. Voltage waveform and harmonic distribution after imposing the disturbance.

so as to produce the harmonic excitation at the controlled bandwidth. Besides, the electrical signals acquisition device is used to measure the data of voltage and current waveforms, and then, processing data by MATLAB to calculate the TPS impedances.

In the measurement process, the desired measured frequency band is first set up by the operator via controlling the minimum and maximum frequencies of the chirp-PWM signal. Thereafter, the butterfly-type disturbance circuit can excite the harmonics at the controlled frequency band, so as to detect the response data of the voltage and current with the electrical signals acquisition device. Finally, the computer can calculate the measured TPS impedances and show them on the screen.

B. Experimental Results

To detect the voltage waveform and background harmonics of the measurement point, they can be seen in Fig. 16. Usually, there are some normal background harmonics (e.g., 5th, 7th, 11th, and 13th harmonics) brought by the traction transformer, utility power system, and some nonlinear devices and it is accordant with actual engineering [2].

The impedances of the specified frequency band considering the impact of background harmonics can be measured via the proposed method mentioned in Sections II and III, and the operator controls the specified frequency band. For instance, the specified frequency band is controlled at 2000–3000 Hz, and Fig. 17 gives the voltage waveform and its harmonic spectrum of the measurement point after imposing the disturbance. The excited harmonics can follow the specified frequency band and the total harmonic distortion (THD) is 9.58% (seen from Fig. 17) rising from the original 3.77% (seen from Fig. 16). The harmonic distortion can be acceptable and does not affect the normal operation of the TPS without electric trains.

Fig. 18 presents the measurement results and the measured impedances at the specified 2000 –3000 Hz frequency band that can match the theoretical value accurately. Therefore, the measured impedance is reasonably accurate under the traditional operations of the traction system. The variations of the THD

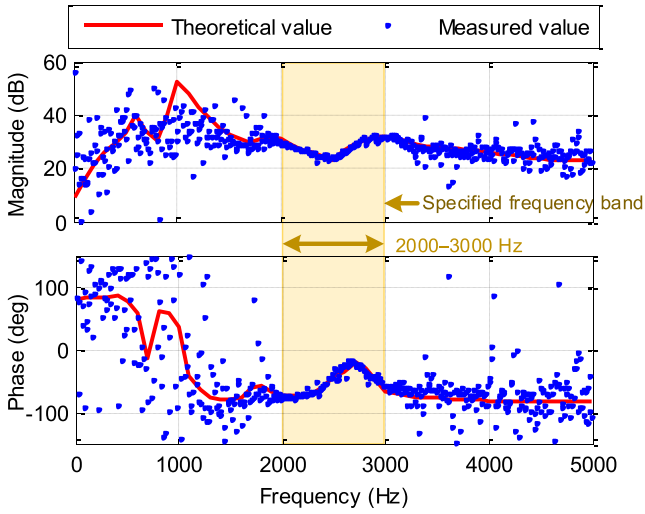

Fig. 18. Measured TPS impedance when the specified frequency band is 2000–3000 Hz.

values also indicate that the disturbance power is neither excessive nor insufficient in measuring the network impedance. It is noted that the disturbance power may not be the most capable one for measuring the network impedance and can be studied further in the future with considering the system damping conditions.

In order to measure the TPS impedance at a broader band 0–5000 Hz, similarly, one can excite the harmonics directly at 0–5000 Hz. However, the exorbitant harmonic excitation may affect the normal operation of the TPS. Thus, we can conduct a segmental injection and measurement, for instance, every 1000 Hz (i.e., specified frequency bands at 0–1000 Hz, 1000–2000 Hz, 2000–3000 Hz, 3000–4000 Hz, and 4000–5000 Hz) using the proposed measurement method for dividing the excited harmonic power.

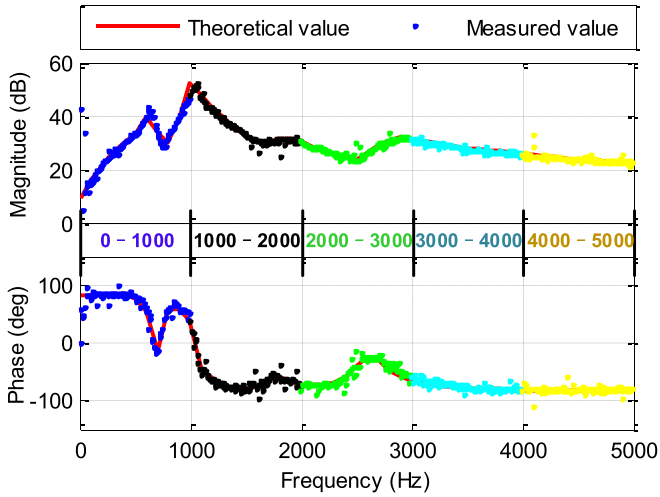

Fig. 19. Measured TPS impedance when the specified frequency band is 0–5000 Hz with 1000-Hz measurement interval.

TABLE III
VALUES OF THREE INDICES FOR EXPERIMENTAL DISTURBANCE

Frequency band	HCR	HDU	HFR
0 – 1000 Hz	0.9640	0.18	10 Hz
1000 – 2000 Hz	0.9044	0.19	10 Hz
2000 – 3000 Hz	0.9416	0.22	10 Hz
3000 – 4000 Hz	0.9608	0.19	10 Hz
4000 – 5000 Hz	0.9814	0.17	10 Hz

Consequently, Fig. 19 gives the measured result, and the accurate impedance at 0–5000 Hz can be obtained via the segmental measurements, which validates the correctness and capability of the proposed measurement method at a specified frequency band. The values of proposed three indices are calculated in Table III. The power of fundamental and harmonics at a specified frequency band is sufficient and can reach over 90% according to the HCR. The spread frequency spectrum at a specified frequency band is uniform with the small HDU values. The HFR is 10 Hz as the sampling time is set as 0.1 s. All of the three indices show that the proposed impedance approach has a suitable disturbance power and achieve a good performance and accuracy under practical conditions.

VI. CONCLUSION

This paper presented an impedance measurement method for the TPS so that the measured frequency band could be controlled. A butterfly-type disturbance circuit consisted of two IGBTs, four uncontrollable diodes, and three adjustable resistors was designed, and the broad harmonic excitation at specified frequency band could be produced by means of the chirp-PWM signal to drive the IGBTs. Three defined indices, namely, HCR, HDU, and HFR, were proposed to evaluate the performance of the disturbance injection. These indices help to determine the values of adjustable resistors of the butterfly-type disturbance circuit for getting a most suitable disturbance. Finally, the TPS impedance can be calculated using the response voltages and currents. The proposed method was verified by simulations and experiments. Applying this technique, the measured frequency band can be controlled more flexibly, and the impedance at desired frequency band can be measured by imposing the disturbance only once that greatly reduces the measurement time.

REFERENCES

[1] M. Brenna, F. Foiadelli, and D. Zaninelli, "New stability analysis for tuning PI controller of power converters in railway application," *IEEE Trans. Ind. Electron.*, vol. 58, no. 2, pp. 533–543, Feb. 2011.
[2] H. Hu, Y. Shao, L. Tang, J. Ma, Z. He, and S. Gao, "Overview of harmonic and resonance in railway electrification systems," *IEEE Trans. Ind. Appl.*, vol. 54, no. 5, pp. 5227–5245, Sep./Oct. 2018.
[3] M. Shafighy, S. Y. Khoo, and A. Z. Kouzani, "Modified DSC propulsion systems for efficient direct recovery of regeneration in 25-kV AC traction power supply," *IEEE Trans. Transport. Electrific.*, vol. 3, no. 3, pp. 632–645, Sep. 2017.
[4] H. Tao, H. Hu, X. Wang, F. Blaabjerg, and Z. He, "Impedance-based harmonic instability assessment in multiple electric trains and traction network interaction system," *IEEE Trans. Ind. Appl.*, vol. 54, no. 5, pp. 5083–5096, Sep./Oct. 2018.
[5] H. Hu *et al.*, "Train-network interactions and stability evaluation in high-speed railways—Part I: Phenomena and modeling," *IEEE Trans. Power Electron.*, vol. 33, no. 6, pp. 4627–4642, Jun. 2018.
[6] H. Hu *et al.*, "Train-network interactions and stability evaluation in high-speed railways—Part II: Influential factors and verifications," *IEEE Trans. Power Electron.*, vol. 33, no. 6, pp. 4643–4659, Jun. 2018.
[7] Y. Liao, Z. Liu, G. Zhang, and C. Xiang, "Vehicle-grid system modeling and stability analysis with forbidden region-based criterion," *IEEE Trans. Power Electron.*, vol. 32, no. 5, pp. 3499–3512, May 2017.
[8] H. Wang, W. Mingli, and J. Sun, "Analysis of low-frequency oscillation in electric railways based on small-signal modeling of vehicle-grid system in dq frame," *IEEE Trans. Power Electron.*, vol. 30, no. 9, pp. 5318–5330, Sep. 2015.
[9] H. Hu *et al.*, "A practical approach to mitigate low-frequency oscillation in railway electrification system," *IEEE Trans. Power Electron.*, vol. 33, no. 10, pp. 8198–8203, Oct. 2018.
[10] Y. Li *et al.*, "A virtual impedance comprehensive control strategy for the controllably inductive power filtering system," *IEEE Trans. Power Electron.*, vol. 32, no. 2, pp. 920–926, Feb. 2017.
[11] Y. Panov and M. M. Jovanovic, "Stability and dynamic performance of current-sharing control for paralleled voltage regulator modules," *IEEE Trans. Power Electron.*, vol. 17, no. 2, pp. 172–179, Mar. 2002.
[12] M. Cespedes and J. Sun, "Adaptive control of grid-connected inverters based on online grid impedance measurements," *IEEE Trans. Sustain. Energy*, vol. 5, no. 2, pp. 516–523, Apr. 2014.
[13] S. Cobreces *et al.*, "Grid impedance monitoring system for distributed power generation electronic interfaces," *IEEE Trans. Instrum. Meas.*, vol. 58, no. 9, pp. 3112–3121, Sep. 2009.
[14] P. Xiao *et al.*, "recurrent neural networks-based impedance measurement technique for power electronic systems," *IEEE Trans. Power Electron.*, vol. 25, no. 2, pp. 382–390, Feb. 2010.
[15] T. Roinila and T. Messo, "Online grid-impedance measurement using ternary-sequence injection," *IEEE Trans. Ind. Appl.*, vol. 54, no. 5, pp. 5097–5103, Sep./Oct. 2018.
[16] J. Huang, K. A. Corzine, and M. Belkhayat, "Small-signal impedance measurement of power-electronics-based ac power systems using line-to-line current injection," *IEEE Trans. Power Electron.*, vol. 24, no. 2, pp. 445–455, Feb. 2009.
[17] B. Wen, D. Boroyevich, R. Burgos, P. Mattavelli, and Z. Shen, "Small-signal stability analysis of three-phase ac systems in the presence of constant power loads based on measured d-q frame impedances," *IEEE Trans. Power Electron.*, vol. 30, no. 10, pp. 5952–5963, Oct. 2015.
[18] M. Jordan, H. Langkowski, T. D. Thanh, and D. Schulz, "Frequency dependent grid-impedance determination with pulsewidth modulation- signals," in *Proc. 7th Int. Conf.-Workshop Compat. Power Electron.*, Jun. 2011, pp. 131–136.
[19] R. Luhtala, T. Messo, T. Reinikka, J. Sihvo, T. Roinila, and M. Vilkko, "Adaptive control of grid-connected inverters based on real-time measurements of grid impedance: DQ-domain approach," in *Proc. IEEE Energy Convers. Congr. Expo.*, Oct. 2017, pp. 69–75.

[20] T. Roinila, T. Messo, and E. Santi, "MIMO-Identification techniques for rapid impedance-based stability assessment of three-phase systems in DQ domain," *IEEE Trans. Power Electron*, vol. 33, no. 5, pp. 4015–4022, May 2018.
[21] T. Roinila, M. Vilkko, and J. Sun, "Online grid impedance measurement using discrete-interval binary sequence injection," *IEEE J. Emerg. Sel. Topics Power Electron.*, vol. 2, no. 4, pp. 985–993, Dec. 2014.
[22] M. Min, R. Land, T. Paavle, T. Parve, P. Annus, and D. Trebbels, "Broadband spectroscopy of dynamic impedances with short chirp pulses," *Physiol. Meas.*, vol. 32, no. 7, pp. 945–958, 2011.
[23] T. Saar, M. Reidla, O. Martens, R. Land, M. Min, and H. Herranen, "Chirp-based piezo-impedance measurement," in *Proc. IEEE 8th Int. Symp. Intell. Signal Process.*, 2013, pp. 83–86.
[24] T. Paavle, M. Min, and D. Trebbels, "Low-energy chirps for bioimpedance measurement," in *Proc. 34th Int. Conf. Telecommun. Signal Process.*, 2011, pp. 398–402.
[25] Z. Shen, M. Jaksic, P. Mattavelli, D. Boroyevich, J. Verhulst, and M. Belkhayat, "Three-phase AC system impedance measurement unit (IMU) using chirp signal injection," in *Proc. 28th Annu. IEEE Appl. Power Electron. Conf. Expo.*, 2013, pp. 2666–2673.
[26] Z. He, H. Hu, and Y. Zhang, "Harmonic resonance assessment to traction power-supply system considering train model in China high-speed railway," *IEEE Tran. Power Del.*, vol. 29, no. 4, pp. 1735–1743, Aug. 2014.
[27] P. Pan, H. Hu, X. Yang, F. Blaabjerg, X. Wang, and Z. He, "Impedance measurement of traction network and electric train for stability analysis in high-speed railways," *IEEE Trans. Power Electron.*, vol. 33, no. 12, pp. 10086–10100, Dec. 2018.
[28] W. Uddin, T. Husain, R. Mitra, E. Ofori, Y. Sozer, and I. Husain, "A chirp PWM scheme for brushless DC motor drives," in *Proc. IEEE Energy Convers. Congr. Expo.*, 2012, pp. 3317–3323.
[29] Q. Liu, Y. Li, S. Hu, and L. Luo, "A controllable inductive power filtering system: Modeling, analysis and control design," *Int. J. Elect. Power Energy Syst.*, vol. 105, pp. 717–728, Feb. 2019.

Haitao Hu (S'13–M'14) received the B.S. degree from Zhengzhou University, Zhengzhou, China, in 2010, and the Ph.D. degree from Southwest Jiaotong University, Chengdu, China, in 2014, both in electrical engineering.

From 2013 to 2014, he was a Visiting Doctoral Scholar with the University of Alberta, Edmonton, AB, Canada. He is currently an Associate Professor with the School of Electrical Engineering, Southwest Jiaotong University. His main research interests include power quality and stability of the electric traction system.

Pengyu Pan (S'17) received the B.S. degree in electrical engineering in 2016 from Southwest Jiaotong University, Chengdu, China, where he is currently working toward the Ph.D. degree in electrical engineering.

His research interests include impedance measurement, stability analysis, and control of power electronic-based power systems including high-speed railways.

Yitong Song received the B.S. degree in electrical engineering in 2018 from Southwest Jiaotong University, Chengdu, China, where she is currently working toward the master's degree in electrical engineering.

Her research interests include the impedance measurement in the field of traction power supply system and high-speed railways.

Zhengyou He (M'10–SM'13) received the B.Sc. and M.Sc. degrees in computational mechanics from Chongqing University, Chongqing, China, in 1992 and 1995, respectively, and the Ph.D. degree in electrical engineering from the School of Electrical Engineering, Southwest Jiaotong University, Chengdu, China, in 2001.

He is currently a Professor with the School of Electrical Engineering, Southwest Jiaotong University. His research interests include signal processing and information theory applied to electrical power system, and the application of wavelet transforms in power systems.